IOP Publishing Prog. Energy 3 (2021) 012001 https://doi.org/10.1088/2516-1083/abd488

Progress in Energy

RECEIVED
25 September 2020

REVISED
26 November 2020

ACCEPTED FOR PUBLICATION
17 December 2020

PUBLISHED
4 February 2021

TOPICAL REVIEW

Review of injection dependent charge carrier lifetime spectroscopy

Yan Zhu* and Ziv Hameiri

School of Photovoltaic and Renewable Energy Engineering, University of New South Wales, Sydney, Australia

* Author to whom any correspondence should be addressed.

E-mail: yan.zhu@unsw.edu.au

Keywords: photovoltaic, charge carriers, lifetime spectroscopy, defect

Abstract

Characterization and identification of recombination active defects in photovoltaic (PV) materials are essential for improving the performance of solar cells, hence, reducing their levelized cost of electricity. Injection dependent lifetime spectroscopy (IDLS) is a sensitive and widely used technique for investigating defects in silicon. With the development of carrier lifetime measurement techniques and analysis methods, IDLS has gained increasing popularity within the PV research community. In this paper, we review IDLS, from measurement techniques and systems, to existing and emerging defect parameterization methods. We also discuss the limitations and potential pitfalls of lifetime spectroscopy analysis and outline the possible approaches for improvement.

1. Introduction

The global cumulative photovoltaic (PV) module installation has increased from around 20 gigawatt-peak (GWp) in 2009 to over 600 GWp in 2019 [1] and the market is primarily dominated by technologies based on crystalline silicon (c-Si) [2]. This tremendous increase is largely contributed by the continuously incremental improvements in c-Si solar cell efficiency (from 12% average module efficiency in 2009 to 17% in 2019 [3]), which significantly lowers the levelized cost of electricity.

For a continuous increase of solar cell efficiency and cost reduction, the improvement of c-Si material quality is essential. In a c-Si solar cell, each absorbed photon with energy above 1.1 eV can excite an electron–hole pair across the semiconductor bandgap. The excited electrons and holes (charge carriers) are then collected from the corresponding electrodes to generate electricity [4]. However, defects add energy levels into the bandgap of semiconductor, which stimulate the recombination of the excited electron–hole pairs and dissipate the energy as heat (mainly). The lifetime of charge carriers (the average time the excited charge carriers exist before recombination) is reduced and the probability to collect them from the electrodes decreases, leading to a decrease of the solar cell efficiency [5, 6]. Therefore, characterization and mitigation of defects has always been one of the main focuses of the PV industry and research community.

With the development and commercialization of advanced solar cell structures, such as passivated emitter and rear cell [7, 8], silicon heterojunction [9], and passivating contacts [10–13], recombination of charge carriers at silicon surfaces and silicon-metal interfaces is largely suppressed. Hence, for these advanced designs, recombination via bulk defects plays a significant role in the overall charge carrier recombination process [14, 15]. Therefore, in order to maximize the benefits of those advanced solar cell structures, minimizing the recombination-active bulk defects is becoming increasingly important [16–18].

Identification of defects is essential for their elimination during crystal growth and solar cell fabrication [16]. Understanding the electrical properties of defects is also important for evaluating their impact on device performance [17, 19]. However, as the quality of silicon continues to improve, the concentration of bulk defects decreases, making their detection more and more challenging. Nevertheless, even in a dilute concentration, some defects still have a significant impact on the charge carrier lifetime [20].

Lifetime spectroscopy refers to the characterization techniques which extract defect parameters from charge carrier lifetime measurements [20]. As long as the recombination induced by a defect dominates the overall charge carrier recombination, lifetime spectroscopy should be highly sensitive to the defect, no matter

what the absolute defect concentration is. This unique characteristic makes lifetime spectroscopy favorable for the characterization of recombination active defects.

Lifetime spectroscopy has different variations depending on the conditions of the measurement [20]. Temperature dependent lifetime spectroscopy (TDLS) involves low injection (when the excess carrier concentration is much smaller than the net doping concentration) lifetime measurements at various temperatures [21, 22]. Injection dependent lifetime spectroscopy (IDLS) involves measuring lifetimes across a range of excess carrier concentrations [23–25]. IDLS with temperature variation is referred to as T-IDLS [26, 27], whereas IDLS with sample doping variation is referred to as N_{dop}-IDLS [28–30].

The early applications of lifetime spectroscopy were predominantly based on TDLS [22, 31, 32]. Later, with the development of the quasi-steady state photoconductance (QSSPC) lifetime measurement technique [33], IDLS started to be applied to defect characterization [25, 34, 35]. However, the spectroscopic potential of lifetime spectroscopy techniques was only revealed by the systematic investigation of Rein *et al* [36], which was discussed in more details in Rein's doctoral dissertation [20]. One of the key findings of Rein's work is that IDLS is ambiguous for the parameterization of a Shockley–Read–Hall (SRH) defect [37, 38]. With IDLS, the defect parameters can only be confined into a solution surface where an infinite number of solutions of the defect parameters exist [20, 36]. T-IDLS and N_{dop}-IDLS reduce the number of solutions to two, the true solution and a false solution with an energy level in the opposite half of the bandgap [20]. Compared to N_{dop}-IDLS, T-IDLS could potentially identify the correct solution, if the ratio of the defect capture cross section is large enough [20].

With the systematic study of Rein *et al* [20, 36], lifetime spectroscopy has grown in popularity. It has been used to characterize the electrical properties of various defects in silicon, such as metal impurities [25, 27, 28, 39–45], oxygen precipitates [29, 46, 47], and process related defects [34, 35, 48–52]. Lifetime spectroscopy has also been used to identify unknown defects by comparing the extracted parameters with reported defect parameters from literature [53–55]. As injection dependent lifetime measurements have been made so convenient, IDLS, T-IDLS and N_{dop}-IDLS have been used more widely than TDLS. Therefore, in this review, we mainly focus on lifetime spectroscopy techniques with injection dependency. Throughout this paper, the term 'injection dependent' refers to 'as a function of excess carrier concetration'.

This paper aims to provide an overview of IDLS, from the measurement to the analysis. Although the studies by Rein *et al* [20, 36] have been widely used as guidelines for lifetime spectroscopy techniques, advances in both lifetime measurements and defect parameterization methods have been made since then. This paper reviews these advances. Moreover, although lifetime spectroscopy seems to be a relatively simple technique compared to other traditional defect characterization techniques, such as deep-level transient spectroscopy (DLTS) [56], there are a few pitfalls that can impact the accuracy of the results and might not be given enough attention. Here, we discuss these pitfalls and other potential limitations of the IDLS-based techniques; we also suggest several possible improvements.

2. Injection dependent lifetime measurement

2.1. Methods of lifetime measurements

For a uniformly distributed, photogenerated excess carrier, its concentration Δn follows the continuity equation [57]:

$$\frac{d\Delta n}{dt} = G - \frac{\Delta n}{\tau(\Delta n)} \tag{1}$$

where t is time, G is the generation rate and τ is the carrier lifetime. The injection dependent lifetime can thus be obtained by exciting the sample with varying G and measuring Δn and G as a function of time:

$$\tau(\Delta n) = \frac{\Delta n(t)}{G(t) - d\Delta n(t)/dt}. \tag{2}$$

If a constant G is used and Δn is measured after stabilization, the time dependent term $d\Delta n/dt$ vanishes. This measurement regime is called the *steady state* condition. In a steady state measurement, the lifetime can only be measured for one injection at a time. Meanwhile, at high excitation light intensity, the constant illumination can heat up the sample, increasing the difficulty of obtaining a measurement at fixed temperature.

If an illumination source that can be abruptly switched off is used and the decay of Δn is measured, the term $G(t)$ in equation (2) vanishes. This measurement regime is called the *transient* condition. The advantage of a transient condition is that $G(t)$ is not required, thus, the measured lifetime does not suffer from the uncertainty in the $G(t)$ measurement.

However, from equation (1) it can be seen that the decay of Δn for samples with lower lifetime is faster. For a transient measurement, this requires a faster response of the measurement system and a more abrupt switch-off of the illumination. Instead, if $G(t)$ varies slowly, the change of Δn will also be slow, no matter what the lifetime is. When $G(t)$ varies slowly enough such that the term $d\Delta n(t)/dt$ is negligible compared to $G(t)$, the measurement condition is referred to as the *quasi-steady-state* (QSS) [33, 58]. The advantage of QSS measurements over transient measurements is that $G(t)$ and $\Delta n(t)$ do not need to be measured with an extremely high sampling rate, even for samples with very low lifetimes. However, it suffers from additional uncertainty from the measurement of $G(t)$ compared to the transient measurements. QSS measurements also reduce the potential sample heating compared to the steady state measurement.

The photo-generation rate $G(t)$ is often obtained using a calibrated light detector along with information regarding the sample optics. The detector (which can be a solar cell or a photodiode (PD)) is used to measure the photon flux of the illumination source. Together with a scaling factor related to the sample's optical absorption, the averaged $G(t)$ over the sample thickness can be obtained for the specific illumination spectrum. The scaling factor can be obtained by directly measuring the absorption, numerical modeling, or matching the lifetime curve measured in the QSS condition to the lifetime curve measured in the transient condition [59], as the latter is not impacted by $G(t)$.

The excess carrier concentration can be obtained from either the photoconductance (PC) [33] or the photoluminescence (PL) [60] of the sample. The PC based measurement is more widely used and Δn is correlated to the PC $\Delta\sigma$ by the following equation:

$$\Delta n = \frac{\Delta\sigma}{q\left(\mu_e + \mu_h\right)W} \tag{3}$$

where q is the elementary charge, μ_e and μ_h are, respectively, the mobility of electrons and holes, and W is the thickness of the wafer. As μ_e and μ_h are both a function of Δn, iteration is required to get the correct value of Δn. Several mobility models for silicon that account for non-zero excess carrier concentration have been proposed [61–64]. It should be noted that the mobility also depends on the doping concentrations, and therefore, information regarding the sample's doping is required for the extraction of Δn from the PC. For silicon, with a single dopant type and without a diffused layer, the doping concentration can be obtained by measuring the conductance of the sample in the dark [59]. However, this fails for compensated silicon as the concentrations of both types of dopants have an impact on the mobilities. Information regarding the concentration of dopants must be obtained using other techniques, such as secondary ion mass spectrometry. For samples with diffused layer(s), it is also difficult to obtain the bulk doping concentration from a single conductance measurement as the measured conductance is impacted by the conductance of both the bulk and the diffusion layer(s) [59].

The WCT-100 and WCT-120 lifetime testers from Sinton Instruments [59] have been two of the most widely used PC-based carrier lifetime measurement systems for silicon wafers. These two systems use an inductively coupled radio-frequency coil to measure the PC. The correlation between the output voltage of the coil and the measured conductance can be calibrated using a set of silicon wafers with known conductivity. These two systems use a xenon flash as the light source, decay rate of which can be adjusted. For samples with lifetime below 200 μs, the decay of the flash can be set to a slower mode (decay time constant of around 2.3 ms) to enable QSS measurements. For samples with high enough lifetime, the flash can be set to a faster decay mode (decay time constant of around 50 μs) to enable measurements in transient conditions.

Apart from the inductive coil used in the Sinton lifetime testers, the PC can also be measured from the change of microwave reflectance from the sample. This is the principle of another widely used lifetime technique, the microwave photoconductance decay (μ-PCD) [65, 66]. μ-PCD is a pure transient measurement. Commercial μ-PCD lifetime testers are available from various companies, such as Semilab [67], Freiberg Instruments [68] etc. The main disadvantage of μ-PCD is that the microwave reflectance is a highly non-linear function of the free carrier concentration [69]. Additional measures need to be taken when measuring carrier lifetime at high Δn.

It should be noted that equation (3) is valid under the assumption of equal excess electron concentration and excess hole concentration. This assumption is not valid if minority carrier traps with high enough concentrations exist in the sample [70]. Due to charge neutrality, the minority carriers trapped in the trap centers lead to extra charge in the majority carrier band, which will be misinterpreted as minority carriers, if equation (3) is used. As a result, an artificially high apparent lifetime is obtained at low excess carrier concentration. This is the so-called trapping effect in PC based lifetime measurements [71, 72]. A 'bias-light' method to correct the artifact from the trapping effect has been proposed for QSSPC measurements [73]. This method is made under the assumption of the steady state condition. However, the trap centers might not be in a steady state condition, even under typical QSSPC measurement conditions [73–75]. Therefore, the assumption behind the correction method needs to be evaluated carefully when being applied.

Another well-known artifact in the PC coil-based lifetime measurement is caused by depletion-region modulation (DRM) [76, 77]. For samples with a *p–n* junction or an inversion layer induced by the surface dielectric charge, the excess carrier build at the edge of the depletion region can also lead to artificially high lifetime at low excess carrier concentration. Therefore, if accurate lifetime at low excess carrier concentration is desired, a *p–n* junction or an inversion layer should be avoided.

An alternative method to determine Δn is to measure the PL emission from the sample [60], using the following equation:

$$A_i \Phi_{PL} = B\left(np - n_i^2\right) = B\left(N_{dop} + \Delta n\right) \cdot \Delta n \tag{4}$$

where A_i is a calibration factor, Φ_{PL} is the PL photon flux emitted from the sample, B is the radiative recombination coefficient, n and p are, respectively, the total free electron and hole concentration, n_i is the intrinsic carrier concentration, and N_{dop} is the net doping concentration.

The calibration of PL to Δn requires knowledge of A_i, which depends not only on the measurement system, but also on the sample. One approach to calibrate a PL-based measurement is to match it with a PC-based measurement at high excess carrier concentration where the PC measurements are not impacted by trapping or DRM. A purely PL-based calibration method, called the self-consistent method [78] has also been proposed to convert the measured PL to Δn. In this method, a modulated (usually sinusoidal) excitation is used and the time dependent $\Phi_{PL}(t)$ is recorded, while $G(t)$ can be calibrated from the photon flux of the excitation source as discussed previously. For a given A_i, $\Delta n(t)$ can be calculated from $\Phi_{PL}(t)$ using equation (4) and $\tau(\Delta n)$ can be calculated using equation (2). The correct value of A_i can be obtained when $\tau(\Delta n)$ from the rising half of $\Phi_{PL}(t)$is consistent with $\tau(\Delta n)$ from the falling half.

The original self-consistent method [78] requires accurate information regarding the net doping concentration as per equation (4). Later, Giesecke *et al* proposed a method to obtain $\tau(\Delta n)$ and the net doping concentration from two PL measurements, one at low excess carrier concentration and the other at intermediate to high concentration [79]. At low excess carrier concentrations, the quadratic term in equation (4) vanishes and the Φ_{PL} is a linear function of Δn. In this case, $\tau(\Delta n)$ calibrated by the self-consistent method is insensitive to N_{dop} as any accuracy in N_{dop} is compensated by A_i. However, for measurements at intermediate to high Δn, $\tau(\Delta n)$ calibrated by the self-consistent method is sensitive to the choice of N_{dop}. Therefore, the correct N_{dop} can be obtained when $\tau(\Delta n)$ from the two measurements coincides.

An alternative PL calibration method named the self-sufficient method, which also does not require information about N_{dop}, was later proposed by Giesecke *et al* [80]. In this method, $\tau(\Delta n)$ is extracted from the time shift between the modulated $G(t)$ and $\Phi_{PL}(t)$. For a sinusoidally modulated $G(t)$, the time shift between the $G(t)$ and PL(t) is related to τ but not strictly equal to τ, due to the injection dependence of τ. Therefore, an iteration procedure is required to extract $\tau(\Delta n)$ from the measured time shift. The details of the self-sufficient method can be found in [80, 81].

The advantage of PL-based lifetime measurements is that they are negligibly impacted by trapping or DRM, even at sensibly low excess carrier concentrations [82]. Moreover, as mentioned previously, PL-based lifetime measurements do not require information about the doping concentration of the sample. In contrast, this information is needed for PC based measurements to calculate the carrier mobilities, which can be complicated for compensated silicon wafers.

It should be highlighted that across this review we assume a uniform distribution of $G(t)$ and $\Delta n(t)$ over the detection area, in both PC and PL measurements. Spatially non-uniform distributions of Δn can have several implications for lifetime measurements. Firstly, G is usually approximated as an average generation rate across the sample thickness. However, strictly speaking G decays exponentially depth-wise in the sample. Using the average generation rate across the sample thickness is acceptable if Δn is uniform across the thickness. This is not the case for non-uniformly distributed Δn. For example, if a sample with a low lifetime (diffusion length much shorter than sample thickness) is illuminated with light of short absorption depth, most of the generated carriers are limited to the region near the front surface. Therefore, in this case, an approximation of G as the average generation rate across the sample thickness can lead to significant error [59]. Secondly, non-uniformly distributed Δn over the detection area only yields a weighted average $\tau(\Delta n)$. Moreover, the average is not the sensitivity weighted arithmetic average of local lifetimes one might intuitively expect. It should be the *intensity* weighted average, as previously discussed [83–85]. Thirdly, the non-uniform distribution of Δn can also lead to a discrepancy in $\tau(\Delta n)$ measured in transient and steady state conditions [86, 87]. This can have a substantial impact on the calibration process which requires time dependent measurements, such as those performed in the self-consistent method. Detailed discussions regarding the non-uniform distribution of Δn in lifetime measurements is out of the scope of this paper; however, it can be found in previous studies [83–87].

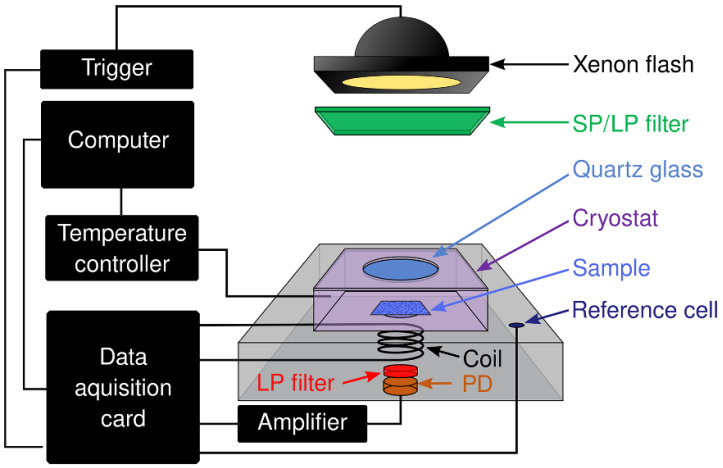

Figure 1. Sketch of the customized lifetime measurement system. The optics for the LED and laser are omitted from the sketch for clarity. SP and LP are shorts for 'short pass' and 'long pass' respectively. PD is short for photodiode.

Spatially resolved techniques can solve the issue of a laterally non-uniform distribution of Δn to some extent. However, the accuracy of the local lifetime extracted from conventional PL imaging is impacted by the lateral carrier flow [88–90]. For non-diffused silicon wafers, the lateral carrier flow can be quantified by calculating the diffusion term in the carrier continuity equation [88]. However, this is not possible for samples with a diffused layer or inversion layer as the lateral carrier flow is dominated by drifting. One potential approach to mitigate this problem is to use PL imaging with adaptive non-uniform illumination to compensate for the lateral non-uniformity in the sample [90]. However, only a proof-of-concept system using this approach has been demonstrated to date.

2.2. Setups of temperature dependent lifetime measurements

The development of carrier lifetime measurement techniques and the aforementioned commercial lifetime testers have greatly facilitated IDLS measurements in silicon. However, a single IDLS is not able to provide accurate defect parameters (this will be discussed in more details in section 3). As IDLS at various temperatures (T-IDLS) can potentially reduce the ambiguity of lifetime spectroscopy analysis [20], lifetime testers with the capability of temperature variation are needed.

A commercial system from Sinton Instruments (WCT-120TS) [91] allows T-IDLS measurements by integrating a hot plate into a standard WCT-120 system. Using this system, measurements from room temperature to 473 K can be done (although the actual sample temperature is usually lower than the stage temperature).

Apart from this commercial lifetime tester, a few systems have been developed in several research institutes. Rein developed a homemade μ-PCD system that used a cryostat allowing measurements from 77 K to 650 K [20]. Giesecke developed a PL based lifetime setup [92] which has been continuously improved over the years [93]. This setup uses a diode laser with a wavelength of around 800 nm as the light source. Reliable PL based lifetime measurements down to the micro-second range have been reported [94]. Recent developments allow measurements between 288 K and 473 K. The system also incorporates PL imaging for spatially resolved lifetime measurements. Electroluminescence imaging has also been integrated to extract resistive information for samples with electrical contacts. Paudyal *et al* presented a customized lifetime tester that was based on a commercial system from Sinton Instruments [95, 96]. This customized system uses a cryostat with a temperature range from 83 K to 673 K.

Recently, the authors developed a customized lifetime tester that allows measurements in a similar temperature range (83 K–673 K) [54, 97]. The main advantage of this new system is the incorporation of a PD to measure the emitted PL signal, thus, it offers simultaneous PC- and PL-based lifetime measurements. Additionally, the system has three different light sources: the standard xenon flash (as of the WCT-120), an 808 nm diode laser and an 810 nm light emitting diode (LED). The three different light sources allow measurements of lifetime over a wide injection range. A sketch of the developed system is shown in figure 1 (the optics associated with the LED and laser are omitted from the sketch for clarity). When the flash is used, a long pass filter is generally employed to allow a more uniform depth-wise degeneration profile in the sample. However, when a PL measurement is required, a short pass filter is used to avoid the illumination light being detected by the PL PD.

3. Lifetime spectroscopy analysis methods

The defect-associated recombination lifetime is a function of defect parameters. For a single-level defect, the most widely accepted recombination lifetime equation is the following SRH lifetime equation [37, 38]:

$$\tau(\Delta n) = \frac{(p_0 + p_1 + \Delta n)/(N_t \sigma_e v_e) + (n_0 + n_1 + \Delta n)/(N_t \sigma_h v_h)}{n_0 + p_0 + \Delta n} \quad (5)$$

where n_0 (p_0) is the electron (hole) concentration at thermal equilibrium, N_t is the defect concentration, $\sigma_e(\sigma_h)$ is the electron (hole) capture cross section, $v_e(v_h)$ is the electron (hole) thermal velocity, $n_1(p_1)$ is the electron (hole) concentration when the Fermi-level is at the defect energy level E_t. Thus, $n_1 = N_C \exp[-(E_C - E_t)/k_B T]$ and $p_1 = N_V \exp[-(E_t - E_V)/k_B T]$, where N_C and N_V are, respectively, the density of states in the conduction and valence band, E_C is the conduction band edge, E_V is the valence band edge, k_B is the Boltzmann constant and T is the temperature.

For a single-level defect following the SRH recombination statistics, its associated defect lifetime can be calculated if N_t and the defect parameters E_t, σ_e and σ_h are known. Lifetime spectroscopy is basically the inverse problem, where we seek the defect parameters from the measured lifetime data.

It should be noted that the measured lifetime is the *effective* lifetime, which involves all the recombination channels in the sample. For lifetime spectroscopy analysis, the defect-associated recombination lifetime needs to be extracted from the measured effective lifetime. This can be done using several approaches. First, one can calculate the recombination rates from the other recombination channels, such as intrinsic and surface recombination, and subtract them from the overall recombination rate [29, 34]. However, the accuracy of the extracted defect-associated lifetime is significantly impacted by how precisely the other rates can be determined and how dominant the defect-associated recombination is. Alternatively, one can intentionally induce defects into a sample to the extent that the defect-associated recombination completely dominates the overall recombination [30]. In this case, the measured effective lifetime essentially equals the defect-associated lifetime. Finally, a control sample without the defect of interest, but with the same other properties as the investigated sample can be used. The defect-associated lifetime can then be obtained by inversely subtracting the lifetimes measured from the investigated and control wafers [98]. The lifetime components related to surface recombination and intrinsic recombination are removed in this approach. However, if the defect-associated recombination does not dominate the overall recombination, the extracted defect-associated lifetime can still suffer from a large uncertainty. For the investigation of metastable defects, the control sample can sometimes be the investigated sample itself prior to the defect activation [50, 51].

After the defect-associated lifetime is extracted from the measured effective lifetime, defect parameters can be extracted using various methods. Here we will give an overview of the different methods.

3.1. Defect parameter solution surface

Among the different analysis methods, the defect parameterization solution space (DPSS) [20] is the most widely used. The details of this method can be found in [20]. Here we demonstrate its principle with a set of simulated lifetime curves. We assume a single-level defect with $E_t = E_C - 0.25\,\text{eV}$, $\sigma_e = \sigma_{e0} T^{-3}$ with $\sigma_{e0} = 5 \times 10^{-7}\,\text{cm}^2$, $\sigma_h = \sigma_{h0} T^{-3}$ with $\sigma_{h0} = 10^{-7}\,\text{cm}^2$, $N_t = 10^{-12}\,\text{cm}^{-3}$, presented in a p-type silicon wafer with a doping concentration of $10^{16}\ \text{cm}^{-3}$. The defect-associated injection dependent lifetime can be calculated using equation (5).

The simulated injection dependent lifetime at three temperatures are shown in figure 2. In this study, the density of states is calculated using the model by Couderc *et al* [99], while the thermal velocity is calculated using the model by Green [100] and the bandgap is calculated with the model of Passle [101] and the bandgap narrowing with the model by Schenk [102].

Each injection dependent lifetime curve can be fitted with equation (5) using three independent variables: E_t, $N_t\sigma_e$ and the ratio of capture cross sections $k = \sigma_e/\sigma_h$. Instead of fitting the three parameters simultaneously, in the DPSS method a value of E_t is assumed and the values of $N_t\sigma_e$ and k are obtained from the optimal fit with this assumed E_t. The value of the assumed E_t is swept within the bandgap, while $N_t\sigma_e$ and k can be obtained from the optimal fit for each assumed E_t. The DPSS curves are then created by plotting the obtained $N_t\sigma_e$ and k as a function of the assumed E_t. The DPSS curves obtained from the simulated lifetime of figure 2 are shown in figure 3. It should be noted that in the original method of Rein [20], $\tau_{e0} = 1/(N_t\sigma_e v_e)$ is used instead of $N_t\sigma_e$. However, as v_e can be considered a known parameter, using the existing model [100], $N_t\sigma_e$ and τ_{e0} are essentially equivalent. Meanwhile, as can be seen from equation (5), σ_e and σ_h are coupled with N_t. It is thus, not possible to extract the absolute value of N_t or the capture cross sections from lifetime spectroscopy, it is only possible to extract their product $N_t\sigma_e$ and $N_t\sigma_h$.

One of the key characteristics of the DPSS curves is that the fitting residuals at any E_t along the DPSS curves are identical. In other words, any combinations of (E_t, $N_t\sigma_e$, k) along the DPSS curves provide the

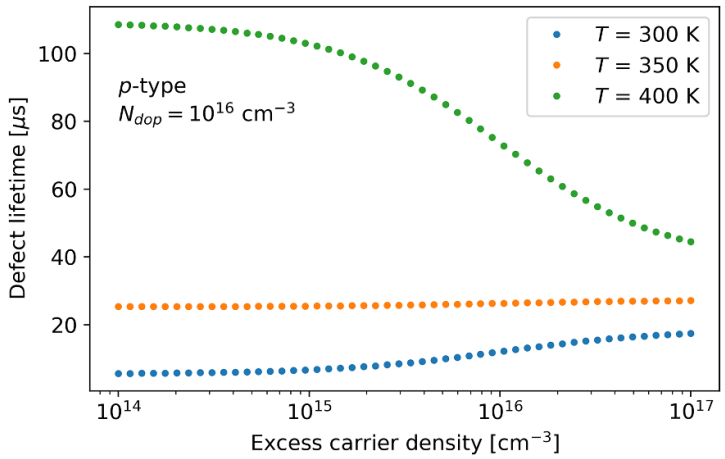

Figure 2. Simulated injection dependent lifetime-associated with a defect in a *p*-type silicon wafer at three temperatures. The parameters of the simulation can be found in text.

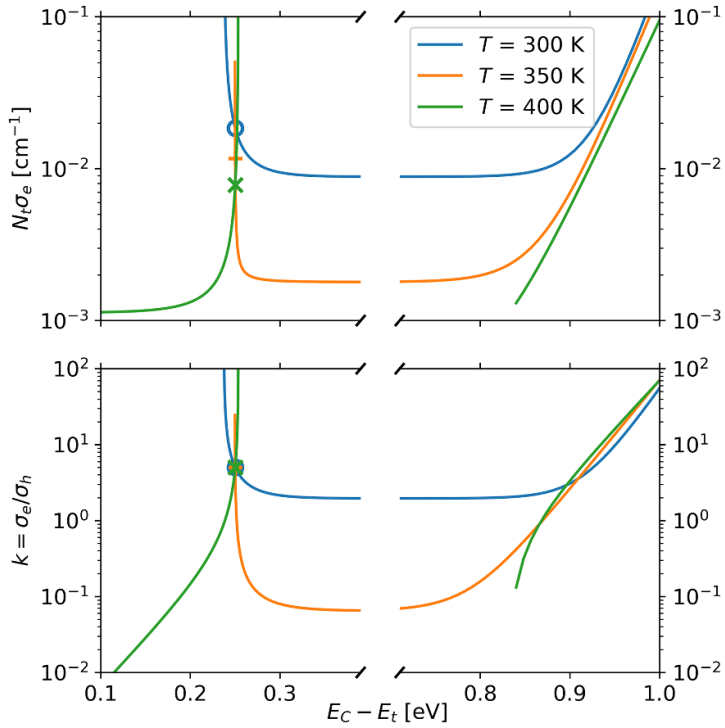

Figure 3. DPSS curves obtained from the simulated injection dependent lifetime curves at three different temperatures. The symbols ('O', '+', and '×') indicate the parameters of the simulated defect. The DPSS curves at 300 K and 350 K are flat in the range 0.4 eV $< E_C - E_t <$ 0.7 eV, therefore, a broken axis is used to gain a better illustration of the DPSS curves closer to the band edges.

same fitting quality to the measured injection dependent lifetime curve. Therefore, from IDLS at a single temperature, it is impossible to determine the correct value of (E_t, $N_t\sigma_e$, k). Only a solution surface which defines all the possible combinations, as illustrated by the DPSS curves, can be obtained.

To reduce the ambiguity in the determination of the defect parameters, IDLS at various temperatures or various doping concentrations is required. In this example, we use the temperature variation. The DPSS curves at different temperatures are plotted together. As can be seen, all the three DPSS curves for k intersect at one point. This point corresponds exactly to the values of E_t and k of the simulated defect. However, the DPSS curves for $N_t\sigma_e$ do not intersect at this E_t. This is not surprising as the simulated σ_e is temperature dependent, whereas k is temperature independent. The value of $N_t\sigma_e$ can be determined at each temperature after the correct E_t is determined from the DPSS curves for k.

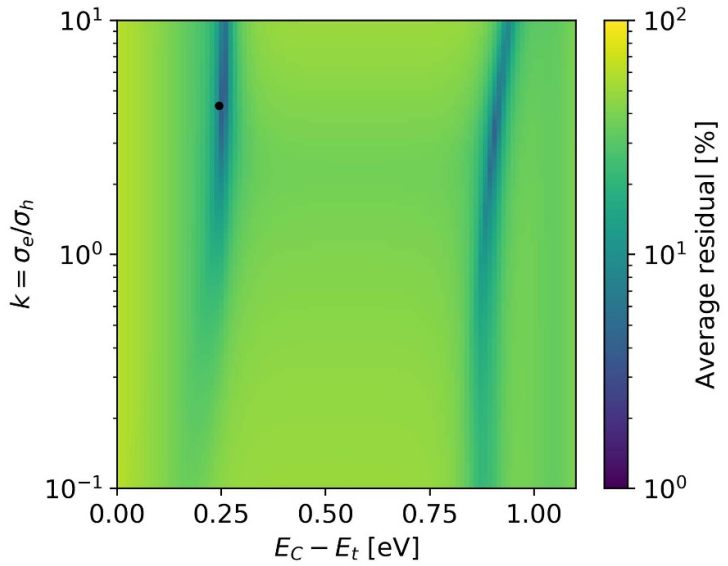

Figure 4. The defect parameter contour map for a set of simulated T-IDLS data. Details of the simulation can be found in the text. The black dot indicates the point with the lowest average residual.

On the lower half of the bandgap, the DPSS curves for k have a set of diffused intersections. These diffused intersections are referred to as the 'fake solution'. As demonstrated by Rein [20], it is possible to distinguish the 'fake solution' from the 'true solution' in T-IDLS if the asymmetry in capture cross sections is large ($k > 10$ or $k < 0.1$) considering the uncertainty in real lifetime measurements. For $0.1 < k < 10$, it is usually difficult to distinguish the two solutions in real measurements.

Here we used T-IDLS as an example, however, DPSS can also be applied to N_{dop}-IDLS. The major difference is that the 'fake solution' will not be more diffused than the 'true solution' in N_{dop}-IDLS, no matter what the value of k is [20]. Therefore, N_{dop}-IDLS always provides two possible solutions for (E_t, $N_t\sigma_e$, k).

As can be seen from figure 3, the DPSS curves at 300 K and 350 K are two continuous curves covering the mid-gap, whereas the DPSS curves at 400 K are two sets of split curves close to the two band edges. It is ideal to have a mix of 'continuous' and 'split' DPSS curves, as the parameterization suffers less from measurement uncertainty compared to the case of only 'continuous' or only 'split' DPSS curves [20]. The transition between the 'continuous' and 'split' DPSS curves occurs when the injection dependency of lifetime changes between increasing and decreasing trends. The critical temperature for T-IDLS (doping level for N_{dop}-IDLS) for this transition can be easily calculated for a given set of defect parameters.

3.2. Defect parameter contour map

A different method of visualization for the defect parameter solution surface has been proposed by Bernardini *et al* [103–105]. In this method (named as defect parameter contour map (DPCM)), a discrete space of (E_t, k) combinations is created. For each (E_t, k) combination, the value of $N_t\sigma_e$ is obtained from the optimal fitting of all the measured injection dependent lifetime data. In the original method, an averaged residual defined as $[\sum_{j=1}^{N}(\sum_{i=1}^{M}|\tau_m - \tau_f|/\tau_m)/M]/N$ is minimized in the fitting procedure, where τ_m is the measured lifetime, τ_f is the modeled lifetime from fitting, M is the number of data points in a single injection dependent lifetime curve, and N is the number of temperatures in T-IDLS (or doping conditions in N_{dop}-IDLS). One can also incorporate the Chi^2 error, as suggested by Rein [20] and Nampalli *et al* [106] to take the measurement uncertainty into consideration. The resulting map of the averaged residual in the (E_t, k) space provides a visualization of the possible solutions for the defect parameters.

A demonstration of the resulting DPCM for a set of simulated lifetime data is shown in figure 4. The sample and defect parameters used for the simulation are identical to the ones used in the DPSS section, except that the capture cross sections are temperature independent, with $\sigma_e = 5 \times 10^{-14}$ cm^2 and $\sigma_h = 10^{-14}$ cm^2. The reason for this adjustment will be discussed below. As can be seen, two bands of low residual can be found in the (E_t, k) space. The DPCM thus provides a clear visualization of the possible combinations of (E_t, k) that can fit the measured lifetime data. The point with the lowest residual value is marked with a black dot and it agrees well with the simulated values of (E_t, k) of the defect. In this ideal scenario, the correct (E_t, k) values are extracted from the DPCM.

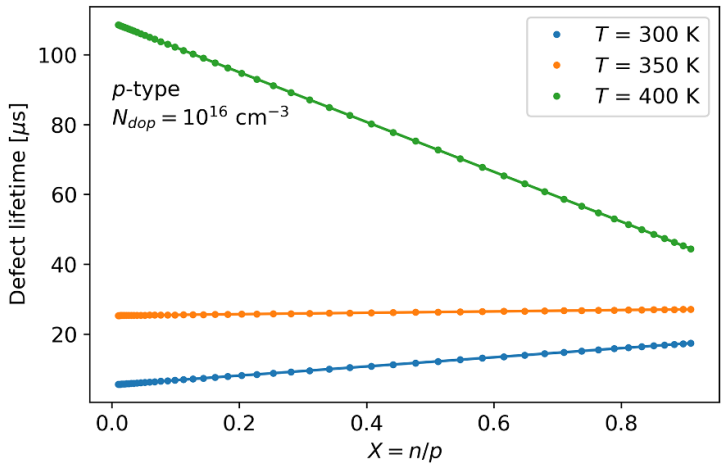

Figure 5. Simulated injection dependent defect lifetime plotted as a function of X at three different temperatures. The details of the simulation can be found in the text. The solid lines indicate the linear fitting of the data.

One major difference between the DPCM and the DPSS is that in the DPCM all the IDLS data are fitted simultaneously, whereas in the DPSS each set of IDLS data is fitted independently. In the DPSS analysis, the defect parameters can be obtained if k is constant for all the measured lifetime data. However, the DPCM analysis also requires $N_t\sigma_e$ (so as $N_t\sigma_h$) to be assumed to be a constant. However, for T-IDLS this assumption is not valid if any of the capture cross section is temperature dependent. For N_{dop}-IDLS, this assumption is also not valid if N_t is different in different samples. An error in the resulting defect parameters can occur due to the invalidity of this assumption. Bernardini *et al* [104] account for this issue by assigning an error to the extracted k value. However, an accurate determination of this error requires knowledge of the temperature dependency of the capture cross sections.

3.3. Methods based on lifetime linearization

Apart from DPSS and DPCM, alternative methods for defect parameterization have been proposed [29, 53, 107]. These methods are based on linearization of the SRH lifetime [29, 108, 109]. For p-type silicon fulfilling $n_0 \ll p_0$ and $n_0 \ll \Delta n$, SRH lifetime in equation (5) can be transformed into a linear form by introducing a variable $X = n/p = (n_0 + \Delta n)/(p_0 + \Delta n)$, where n and p are the total free electron and hole concentration, respectively:

$$\tau(X) = \frac{\left[\left(1 + \frac{kn_1\nu_e}{p_0\nu_h} + \frac{p_1}{p_0}\right) + \left(\frac{k\nu_e}{\nu_h} - \frac{kn_1\nu_e}{p_0\nu_h} - \frac{p_1}{p_0}\right)X\right]}{N_t\sigma_e\nu_e} \tag{6}$$

An illustration of this linearization process is made in figure 5, where the simulated lifetime of figure 2 is now plotted against X. As can be seen, the lifetime curves are now linear. Therefore, each set of IDLS data can be simply fitted as a straight line, with the slope m and intercept b, both functions of (E_t, $N_t\sigma_e$, k):

$$\begin{cases} m = \left(\frac{k}{\nu_h} - \frac{kn_1}{p_0\nu_h} - \frac{p_1}{p_0\nu_e}\right)/N_t\sigma_e \\ b = \left(\frac{1}{\nu_e} + \frac{kn_1}{p_0\nu_h} + \frac{p_1}{p_0\nu_e}\right)/N_t\sigma_e \end{cases} \tag{7}$$

Based on this linearization, Murphy *et al* [29] proposed a method to extract defect parameters from N_{dop}-IDLS. Equation (7) can be transformed to:

$$\begin{cases} \frac{m}{m+b} = \frac{k}{k+\nu_h/\nu_e} - \frac{1}{p_0}\left(\frac{kn_1+p_1\nu_h/\nu_e}{k+\nu_h/\nu_e}\right) \\ b = \left[\frac{1}{\nu_e} + \frac{1}{p_0}\left(\frac{kn_1+p_1\nu_h/\nu_e}{\nu_h/\nu_e}\right)\right]/N_t\sigma_e \end{cases} \tag{8}$$

As can be seen, $m/(m+b)$ and b are both a linear function of $1/p_0$. From a linear fitting of $m/(m+b)$ against $1/p_0$, the value of k can be extracted from the intercept. With the value of k, $kn_1 + p_1\nu_h/\nu_e$ can be extracted from the slope. From a linear fitting of b against $1/p_0$, the value of $N_t\sigma_e$ can be extracted either from the intercept or from the slope (with the information of $kn_1 + p_1\nu_h/\nu_e$). With the value of k and $kn_1 + p_1\nu_h/\nu_e$, E_t can be determined. However, for any value of$kn_1 + p_1\nu_h/\nu_e$, there are always two possible

values for E_t, as the product of $n_1 p_1$ is a constant equal to n_i^2. Subsequently, to determine the correct E_t from these two possible solutions, temperature dependent lifetime data is required. This is similar to the two intersections in the DPSS method.

The method of Murphy *et al* was developed for N_{dop}-IDLS. Later on, Morishige and Jensen *et al* [53] adapted the concept of linearization to the DPSS method, and makes it applicable for both N_{dop}-IDLS and T-IDLS. The equation for m and b (equation (7)) can also be transformed to:

$$\begin{cases} k = \frac{m/(m+b)+p_1/p_0}{1-n_1/p_0-m/(m+b)} \frac{\nu_h}{\nu_e} \\ N_t\sigma_e = \left[\frac{1}{\nu_e} + \frac{1}{p_0}\left(\frac{kn_1+p_1\nu_h/\nu_e}{\nu_h/\nu_e}\right)\right]/b \end{cases} \tag{9}$$

As can be seen, k is now expressed as a function of m, b, E_t and other parameters that can be calculated from existing models. Therefore, when m and b are obtained from the linear fit, k can be calculated with any assumed value of E_t. The value of $N_t\sigma_e$ can also be easily obtained with any assumed value of E_t after the calculation of k. The DPSS curves can be easily obtained by calculating k and $N_t\sigma_e$, while sweeping E_t within the bandgap.

This method greatly simplifies the original DPSS method. There is no need to fit the lifetime curve at each assumed value of E_t. Instead, only one fit of the linearized lifetime is required and the whole DPSS curves can be obtained from a simple calculation using the fitted slope and intercept.

Another approach to extract (E_t, $N_t\sigma_e$, k) is to consider equation (7) as a system of two equations for three unknown parameters. Since the number of unknown parameters is larger than the number of equations, there are an infinite number of solutions. This provides a mathematical explanation of the ambiguity of a single IDLS. By combining IDLS from two temperatures or two doping conditions, the number of equations becomes four and exceeds the number of unknowns. Therefore, a unique solution can be obtained using, for example, the Newton–Raphson method [110], as demonstrated by Zhu *et al* [107]. However, similarly to the reason explained above, there are always two possible values for E_t in N_{dop}-IDLS. Since this approach attempts to find a single set of (E_t, $N_t\sigma_e$, k) for all IDLS data, similar to DPCM, this method also suffers from errors if $N_t\sigma_e$ or k are not constants for different IDLS data.

Although the above discussions are for p-type silicon, an analogous analysis can be easily made for n-type wafers.

3.4. More recent IDLS analysis methods

More recently, Buratti *et al* proposed a new method for IDLS parameterization using machine learning [111]. By training machine learning algorithms with simulated SRH lifetime data, the method can predict defect parameters with similar accuracy as the human involved methods.

Spatially resolved temperature and IDLS has also been attempted by measuring PL images at various temperatures [112–115]. However, one needs to carefully evaluate the impact of lateral carrier flow on the accuracy of T-IDLS data extracted from an individual pixel of the PL images [88–90].

4. Limitations of lifetime spectroscopy

As presented above, different parameterization methods have been proposed for IDLS analysis. Each of these methods have their own advantages and disadvantages. However, there are a few fundamental limitations for IDLS which applies to all these methods. Ignoring these limitations can cause errors in the resulting defect parameter values.

4.1. Extraction of defect-associated lifetime

The accuracy of IDLS analysis strongly depends on the precision the defect-associated lifetime extracted from the measured sample lifetime. Previously, several approaches to extract the defect lifetime have been discussed. It is worth highlighting again that the accuracy of this extraction process is largely impacted by the dominancy of the defect-associated recombination. If the defect-associated recombination only makes up a small portion of the overall recombination in the sample, the uncertainty in the lifetime measurement will be greatly amplified in the defect associated lifetime extraction process.

Moreover, defects can have a non-uniform distribution within the detection area of the lifetime measurements, for example, in the cases of multi-crystalline silicon, or ring defects in Czochralski silicon [116]. This will lead to a non-uniform distribution of Δn, which can impact the accuracy of the lifetime measurements as discussed in section 2.1.

The metastability of defects can also impact the accuracy of the extraction of defect associated lifetime. For example, iron-boron pairs (FeB) can dissociate into isolated interstitial iron (Fe_i) under excess carrier injection [117]. FeB and Fe_i are both recombination active in p-type silicon and feature significantly different

injection dependent recombination lifetime [118]. Therefore, in the IDLS analysis of FeB, one needs to monitor the FeB dissociation during the measurement. Even if the interested defect is not metastable, it is important to minimize the impact of other potential metastable defects in the sample. Special care needs to be given during temperature dependent measurements. Many metastable defects (e.g. chromium–boron pair [119], light and elevated temperature induced degradation [120] etc) change their states at elevated temperatures. The temperature and measurement duration need to be carefully selected such that the interested defect does not change during the measurement itself. Apart from the defect, it is important to verify that the surface passivation quality is stable throughout the temperature dependent measurements.

4.2. Temperature dependencies of capture cross sections

As can be concluded from the previous discussion, the temperature dependency of the capture cross sections causes problems for T-IDLS analysis. In the above demonstration of the DPSS method, it seems that the defect parameters can be accurately extracted, even if the capture cross sections are temperature dependent. However, it should be noted that in this simulation, σ_e and σ_h are set to have the same temperature dependency. Thus, k is temperature independent. As k is constant, the defect parameters can be extracted from the intersections of DPSS curves for k. Nevertheless, most of the defects whose temperature dependency of capture cross sections have been previously determined have different temperature dependencies for σ_e and σ_h [16, 121, 122]. Therefore, in most cases it is not proper to use the intersection of the DPSS curves for k as an indication of the true defect parameters, unless σ_e and σ_h have been determined to have the same temperature dependency via other techniques.

Compared to T-IDLS, N_{dop}-IDLS does not suffer from the problem of temperature dependency of capture cross sections. However, the main disadvantage of N_{dop}-IDLS is that it requires samples with different doping concentrations while the lifetime of all the samples still needs to be dominated by the same defect.

A potential way to minimize the impact of the temperature dependencies of the capture cross sections in T-IDLS is to combine information from other measurement techniques. For example, if the information about the defect energy level or the capture cross section of majority carriers can be obtained from DLTS, the analysis of IDLS data can then be greatly simplified to extract the information of the minority carrier capture cross section (thus, the defect can be fully parameterized), which is usually more difficult to obtain through DLTS.

4.3. Two-level defects

All the methods discussed in section 3 are based on the SRH recombination statistics, which assumes that the defect has a single energy level within the bandgap. However, in reality, most of the characterized defects have two or more energy levels [122]. The recombination of multi-level defects follows the Sah–Shockley recombination statistics [123], thus, all previous methods might not be able to accurately extract the parameters of two-level defects (or defects with more than two energy levels).

Moreover, in the majority real-life IDLS analysis, the measured injection dependent lifetime curves cannot be fitted with a single SRH defect with a satisfying fitting quality [26, 35, 36, 41, 48, 49, 98, 124–126]. An easier way to examine the fitting quality via a single SRH defect is to use the SRH lifetime linearization presented in section 3. If the measured $\tau - X$ plot can be well fitted with a straight line, it indicates that the defect lifetime is most likely to be dominated by a single defect level. However, if the measured $\tau - X$ plot is a curve, it indicates that the defect lifetime is dominated by more than one defect level, and fitting of the lifetime curve with a SRH defect will, of course, result a bad fitting quality. In most of the previous IDLS analyses, when this occurs, a secondary SRH defect is assumed to be present in the sample. Fitting of the lifetime with two SRH defects usually greatly improves the fitting quality of the measured lifetime curves. The two SRH defects can then be analyzed separately using the methods described in section 3.

However, the curvature of the $\tau - X$ plot can also be explained by a two-level defect [29]. In figure 6, the recombination lifetime of a two-level defect calculated using the Sah–Shockley statistics is plotted against X. As can be seen, a concave curve is obtained. If such lifetime data is measured, it might be interpreted as a result of two single-level defects. In figure 6, the simulated two-level defect recombination lifetime is fitted with two single-level defects. As can be seen, a good fit quality is obtained, however, the model used to fit the data is completely wrong. In this case, the two-level defect is misinterpreted as two single-level defects.

It has been demonstrated previously by Zhu *et al* [127, 128] that misinterpreting a two-level defect as two single-level defects can result in a significant error in the defect parameterization of the IDLS analysis (although not always). By utilizing the $\tau - X$ plot, it has also been shown that it is possible to distinguish the case of a two-level defect from the case of two single-level defects [128]. For two single-level defects, the overall defect lifetime is the harmonic sum of the lifetime from the two defects: $\tau = 1/(1/\tau_{defect\,1} + 1/\tau_{defect\,2})$. In the $\tau - X$ plot, this always leads to a concave curve, as the harmonic sum of two straight lines must be a concave curve. For the case of a two-level defect, the $\tau - X$ plot can either be a

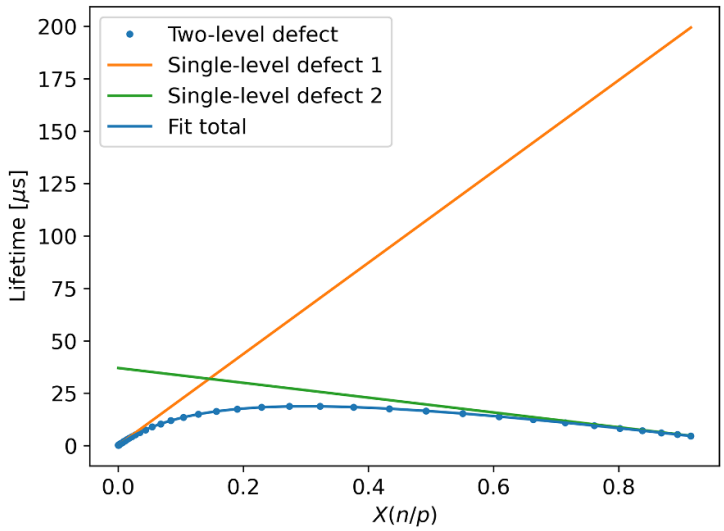

Figure 6. Simulated injection dependent defect lifetime plotted as a function of X for a two-level defect in a p-type sample with doping of 10^{16} cm^{-3} at 300 K. The solid lines indicate the fitting of the simulated lifetime assuming two single-level defects. The simulated two-level defect has a N_t of 10^{12} cm^{-3}, E_t of $E_V + 0.46$ eV, σ_e of 2×10^{-13} cm^2, and σ_e of 10^{-14} cm^2 for the first defect level, and a E_t of $E_V + 0.11$ eV, σ_e of 4×10^{-14} cm^2, and σ_e of 10^{-13} cm^2 for the second defect level.

concave or convex curve, depending on the defect parameters, sample doping level and measurement temperature. Therefore, if a concave $\tau - X$ plot is obtained from measurements, both the case of two single-level defects and the case of a two-level defect need to be considered, if no other information of the defects is available. If a convex $\tau - X$ plot is obtained, it is then certain that the assumption of two single-level defects is not correct and two-level defect parameterization is more suitable in this case. A proper procedure for a two-level defect parameterization in IDLS has also been proposed [128].

4.4. More than two defect levels

In the previous section, we discussed the cases of two single-level defects or a two-level defect. However, it is possible that a more complicated scenario exists. For example, the lifetime is impacted by three or more SRH defects, or by a single-level defect and a two-level defect etc. As discussed, it is easy to determine if the lifetime is dominated by a single-level defect or not (by checking the linearity of $\tau - X$ plot). However, it is more challenging to determine how many defect levels should be used to fit the measured lifetime if the $\tau - X$ plot is not linear. One approach is to use the minimal number of defect levels that provide a satisfying fit of the measured lifetime. However, there is no guarantee that this reflects reality. It is thus essential to have well designed samples for IDLS analysis. For example, by using intentionally contaminated samples and control samples, one can have a better idea of the defects to be investigated. For an unknown system where the origin or chemical nature of the defects is unknown, one needs to be very careful when interpreting the results from IDLS analysis.

Meanwhile, how accurately the defect parameters can be extracted from IDLS when multiple defect levels exist has not been investigated systematically. For the simple case where the measured lifetime is impacted by two single-level defects, if one of the defect dominates the lifetime at middle to low excess carrier concentrations whereas the other one only impacts the lifetime at high excess carrier concentration, it has been shown by Rein that the parameters of the defect dominating the lifetime at middle to low excess carrier concentration can be extracted accurately from IDLS [20]. However, for more general cases or more complicated cases, the error propagation from the measured lifetime to the extracted defect parameters has not been investigated quantitatively. As a rule of thumb, one can expect that the more a defect dominates the overall effective lifetime, the less uncertainty it suffers in the parameterization.

5. Summary

IDLS is a useful technique for the parameterization of recombination active defects. It has been used for the characterization of various defects in silicon and its popularity continues to grow. In this paper, we reviewed this technique from the point of view of the measurements, analysis methods, recent advances as well as its limitations.

We first reviewed the principle of lifetime measurements and introduced the commercial measurement systems of injection dependent lifetime for silicon wafers. Furthermore, a few customized systems allowing temperature dependent measurements, and/or involving different lifetime measurement techniques have been developed in different research institutes.

We then reviewed the analysis methods of IDLS. DPSS is the most widely used method for the parameterization of single-level defects via IDLS techniques. The SRH lifetime linearization technique greatly simplifies the DPSS method. Alternative methods such as DPCM and the Newton–Raphson method have also been proposed.

In the end, we pointed out the limitations and potential pitfalls of IDLS: (a) It is important to evaluate the uncertainties in the defect-associated recombination lifetime extracted from the measured effective lifetime. (b) For T-IDLS analysis, it is important to consider the impact of temperature dependencies of capture cross sections. Combining with other techniques or using N_{dop}-IDLS can mitigate this problem. (c) When the measured lifetime cannot be well fitted with a single-level defect, it is important to consider the possibility of a two-level defect. (d) The capability of resolving more than two defect levels via IDLS is still questionable, therefore, it is important to have well designed experiments to minimize the number of defects in the investigated samples.

Acknowledgments

This work is funded by Australian Government through the Australian Centre for Advanced Photovoltaics (ACAP, project RG200768-G) and the Australian Renewable Energy Agency (ARENA; Projects 2017/RND001 and 2020/RND016). The views expressed herein are not necessarily the views of the Australian Government, and the Australian Government does not accept responsibility for any information or advice contained herein.

ORCID iDs

Yan Zhu https://orcid.org/0000-0002-3672-7127
Ziv Hameiri https://orcid.org/0000-0002-2934-4478

References

[1] IEA PVPS 2020 Snapshot of Global PV Market - *Technical Report* (International Energy Agency (IEA)) (https://iea-pvps.org/snapshot-reports/snapshot-2020/)
[2] VDMA 2019 International Technology Roadmap for Photovoltaic (ITRPV) - *Technical Report* (VDMA) (http://itrpv.vdma.org/download)
[3] Philipps S and Warmuth W 2020 *Photovoltaics Report* (Freiburg: Fraunhofer ISE)
[4] Würfel P and Würfel U 2009 *Physics of Solar Cells: From Basic Principles to Advanced Concepts* (New York: Wiley)
[5] Green M A 1982 *Solar Cells: Operating Principles, Technology, and System Applications* (Sydney: UNSW Press)
[6] Green M A 1995 *Silicon Solar Cells: Advanced Principles and Practice* (Sydney: Centre for Photovoltaic Devices and Systems, University of New South Wales)
[7] Blakers A W, Wang A, Milne A M, Zhao J and Green M A 1989 22.8% efficient silicon solar cell *Appl. Phys. Lett.* **55** 1363–5
[8] Green M A 2015 The passivated emitter and rear cell (PERC): from conception to mass production *Sol. Energy Mater. Sol. Cells* **143** 190–7
[9] Yoshikawa K *et al* 2017 Silicon heterojunction solar cell with interdigitated back contacts for a photoconversion efficiency over 26% *Nat. Energy* **2** 17032
[10] Feldmann F, Bivour M, Reichel C, Hermle M and Glunz S W 2014 Passivated rear contacts for high-efficiency n-type Si solar cells providing high interface passivation quality and excellent transport characteristics *Sol. Energy Mater. Sol. Cells* **120** 270–4
[11] Lozac'h M, Nunomura S and Matsubara K 2020 Double-sided TOPCon solar cells on textured wafer with ALD SiOx layer *Sol. Energy Mater. Sol. Cells* **207** 110357
[12] Yan D, Phang S P, Wan Y, Samundsett C, Macdonald D and Cuevas A 2019 High efficiency n-type silicon solar cells with passivating contacts based on PECVD silicon films doped by phosphorus diffusion *Sol. Energy Mater. Sol. Cells* **193** 80–84
[13] Duttagupta S, Nandakumar N, Padhamnath P, Buatis J K, Stangl R and Aberle A G 2018 MonoPoly^{TM} cells: large-area crystalline silicon solar cells with fire-through screen printed contact to doped polysilicon surfaces *Sol. Energy Mater. Sol. Cells* **187** 76–81
[14] Coletti G 2012 Sensitivity of state-of-the-art and high efficiency crystalline silicon solar cells to metal impurities *Prog. Photovolt., Res. Appl.* **15** 1163–70
[15] Richter A, Benick J, Fell A, Hermle M and Glunz S W 2018 Impact of bulk impurity contamination on the performance of high-efficiency *n*-type silicon solar cells *Prog. Photovolt., Res. Appl.* **26** 342–50
[16] Graff K 2013 *Metal Impurities in Silicon-Device Fabrication* vol 24 (Berlin: Springer)
[17] Coletti G 2011 Impurities in silicon and their impact on solar cell performance *PhD Thesis* University of Utrecht, Utrecht
[18] Davis J R Jr , Rohatgi A, Hopkins R H, Blais P D, Rai-Choudhury P, Mccormick J R and Mollenkopf H C 1980 Impurities in silicon solar cells *IEEE Trans. Electron Devices* **27** 677–87
[19] Schmidt J, Lim B, Walter D, Bothe K, Gatz S, Dullweber T and Altermatt P P 2012 Impurity-related limitations of next-generation industrial silicon solar cells *38th IEEE Photovoltaic Specialists Conf.* pp 1–5

[20] Rein S 2006 *Lifetime Spectroscopy: A Method of Defect Characterization in Silicon for Photovoltaic Applications* vol 85 (Berlin: Springer)
[21] Kirino Y, Buczkowski A, Radzimski Z J, Rozgonyi G A and Shimura F 1990 Noncontact energy level analysis of metallic impurities in silicon crystals *Appl. Phys. Lett.* **57** 2832–4
[22] Hayamizu Y, Hamaguchi T, Ushio S, Abe T and Shimura F 1991 Temperature dependence of minority-carrier lifetime in iron-diffused p-type silicon wafers *J. Appl. Phys.* **69** 3077–81
[23] Ferenczi G, Pavelka T and Tüttô P 1991 Injection level spectroscopy: a novel non-contact contamination analysis technique in silicon *Japan. J. Appl. Phys.* **30** 3630–3
[24] Horaźnyi T S 1996 Identification possibility of metallic impurities in p-type silicon by lifetime measurement *J. Electrochem. Soc.* **143** 216
[25] Walz D, Joly J P and Kamarinos G 1996 On the recombination behaviour of iron in moderately boron-doped p-type silicon *Appl. Phys.* A **62** 345–53
[26] Schmidt J 2003 Temperature- and injection-dependent lifetime spectroscopy for the characterization of defect centers in semiconductors *Appl. Phys. Lett.* **82** 2178–80
[27] Birkholz J E, Bothe K, Macdonald D and Schmidt J 2005 Electronic properties of iron-boron pairs in crystalline silicon by temperature-and injection-level-dependent lifetime measurements *J. Appl. Phys.* **97** 103708
[28] Macdonald D and Cuevas A 2001 Lifetime spectroscopy of FeB pairs in silicon *11th Workshop of Crystalline Silicon Solar Cell Materials and Processes* pp 24–31
[29] Murphy J D, Bothe K, Krain R, Voronkov V V and Falster R J 2012 Parameterisation of injection-dependent lifetime measurements in semiconductors in terms of Shockley-Read-Hall statistics: an application to oxide precipitates in silicon *J. Appl. Phys.* **111** 113709
[30] Sun C, Rougieux F E and Macdonald D 2014 Reassessment of the recombination parameters of chromium in n- and p-type crystalline silicon and chromium-boron pairs in p-type crystalline silicon *J. Appl. Phys.* **115** 214907
[31] Shimura F, Okui T and Kusama T 1990 Noncontact minority-carrier lifetime measurement at elevated temperatures for metal-doped Czochralski silicon crystals *J. Appl. Phys.* **67** 7168–71
[32] Kaniava A, Rotondaro A L P, Vanhellemont J, Menczigar U and Gaubas E 1995 Recombination activity of iron-related complexes in silicon studied by temperature dependent carrier lifetime measurements *Appl. Phys. Lett.* **67** 3930
[33] Sinton R A, Cuevas A and Stuckings M 1996 Quasi-steady-state photoconductance, a new method for solar cell material and device characterization *25th IEEE Photovoltaic Specialists Conf.* pp 457–60
[34] Schmidt J, Berge C and Aberle A G 1998 Injection level dependence of the defect-related carrier lifetime in light-degraded boron-doped Czochralski silicon *Appl. Phys. Lett.* **73** 2167–9
[35] Schmidt J and Cuevas A 1999 Electronic properties of light-induced recombination centers in boron-doped Czochralski silicon *J. Appl. Phys.* **86** 3175–80
[36] Rein S, Rehrl T, Warta W and Glunz S W 2002 Lifetime spectroscopy for defect characterization: systematic analysis of the possibilities and restrictions *J. Appl. Phys.* **91** 2059–70
[37] Shockley W and Read W T 1952 Statistics of the recombination of holes and electrons *Phys. Rev.* **87** 835–42
[38] Hall R N 1952 Electron-hole recombination in germanium *Phys. Rev.* **87** 387–387
[39] Rein S and Glunz S W 2005 Electronic properties of interstitial iron and iron-boron pairs determined by means of advanced lifetime spectroscopy *J. Appl. Phys.* **98** 113711
[40] Diez S, Rein S, Roth T and Glunz S W 2007 Cobalt related defect levels in silicon analyzed by temperature- and injection-dependent lifetime spectroscopy *J. Appl. Phys.* **101** 033710
[41] Rosenits P, Roth T, Glunz S W and Beljakowa S 2007 Determining the defect parameters of the deep aluminum-related defect center in silicon *Appl. Phys. Lett.* **91** 122109
[42] Roth T, Rüdiger M, Warta W and Glunz S W 2008 Electronic properties of titanium in boron-doped silicon analyzed by temperature-dependent photoluminescence and injection-dependent photoconductance lifetime spectroscopy *J. Appl. Phys.* **104** 074510
[43] Paudyal B B, McIntosh K R and Macdonald D H 2009 Temperature dependent carrier lifetime studies on Ti-doped multicrystalline silicon *J. Appl. Phys.* **105** 124510
[44] Sun C, Liu A, Rougieux F E and Macdonald D 2015 Lifetime spectroscopy and hydrogenation of chromium in n-and p-type Cz Silicon *Energy Proc.* **77** 646–50
[45] Inglese A, Lindroos J, Vahlman H and Savin H 2016 Recombination activity of light-activated copper defects in p-type silicon studied by injection- and temperature-dependent lifetime spectroscopy *J. Appl. Phys.* **120** 125703
[46] Murphy J D, Bothe K, Voronkov V V and Falster R J 2013 On the mechanism of recombination at oxide precipitates in silicon *Appl. Phys. Lett.* **102**
[47] Murphy J D, McGuire R E, Bothe K, Voronkov V V and Falster R J 2014 Minority carrier lifetime in silicon photovoltaics: the effect of oxygen precipitation *Sol. Energy Mater. Sol. Cells* **120** 402–11
[48] Rein S and Glunz S W 2003 Electronic properties of the metastable defect in boron-doped Czochralski silicon: unambiguous determination by advanced lifetime spectroscopy *Appl. Phys. Lett.* **82** 1054–6
[49] Bothe K and Schmidt J 2006 Electronically activated boron-oxygen-related recombination centers in crystalline silicon *J. Appl. Phys.* **99** 013701
[50] Niewelt T, Schön J, Broisch J, Warta W and Schubert M 2015 Electrical characterization of the slow boron oxygen defect component in Czochralski silicon *Phys. Status Solidi* **9** 692–6
[51] Niewelt T, Mägdefessel S and Schubert M C 2016 Fast *in-situ* photoluminescence analysis for a recombination parameterization of the fast BO defect component in silicon *J. Appl. Phys.* **120**
[52] Zhu Y, Rougieux F, Grant N, Mullins J, De Guzman J A, Murphy J D, Markevich V P, Coletti G, Peaker A R and Hameiri Z 2019 New insights into the thermally activated defects in n-type float-zone silicon *AIP Conf. Proc.* 2147 140014
[53] Morishige A E, Jensen M A, Needleman D B, Nakayashiki K, Hofstetter J, Li T A and Buonassisi T 2016 Lifetime spectroscopy investigation of light-induced degradation in p-type multicrystalline silicon PERC *IEEE J. Photovolt.* **6** 1466–72
[54] Vargas C, Zhu Y, Coletti G, Chan C, Payne D, Jensen M and Hameiri Z 2017 Recombination parameters of lifetime-limiting carrier-induced defects in multicrystalline silicon for solar cells *Appl. Phys. Lett.* **110** 092106
[55] Vargas C, Coletti G, Chan C, Payne D and Hameiri Z 2019 On the impact of dark annealing and room temperature illumination on p-type multicrystalline silicon wafers *Sol. Energy Mater. Sol. Cells* **189** 166–74
[56] Lang D V 1974 Deep-level transient spectroscopy: a new method to characterize traps in semiconductors *J. Appl. Phys.* **45** 3023–32

[57] Nagel H, Berge C and Aberle A G 1999 Generalized analysis of quasi-steady-state and quasi-transient measurements of carrier lifetimes in semiconductors *J. Appl. Phys.* **86** 6218–21
[58] Sinton R A and Cuevas A 1996 Contactless determination of current–voltage characteristics and minority-carrier lifetimes in semiconductors from quasi-steady-state photoconductance data *Appl. Phys. Lett.* **69** 2510–2
[59] Sinton Instruments 2011 *WCT-120 Photoconductance Lifetime Tester: User Manual* (Boulder, CO: Sinton Instruments)
[60] Trupke T and Bardos R A 2005 Photoluminescence: a surprisingly sensitive lifetime technique *31st IEEE Photovoltaic Specialists Conf.* pp 903–6
[61] Dorkel J M and Leturcq P 1981 Carrier mobilities in silicon semi-empirically related to temperature, doping and injection level *Solid State Electron.* **24** 821–5
[62] Klaassen D B M 1992 A unified mobility model for device simulation—I. Model equations and concentration dependence *Solid State Electron.* **35** 953–9
[63] Klaassen D B M 1992 A unified mobility model for device simulation—II. Temperature dependence of carrier mobility and lifetime *Solid State Electron.* **35** 961–7
[64] Schindler F, Forster M, Broisch J, Schön J, Giesecke J, Rein S, Warta W and Schubert M C 2014 Towards a unified low-field model for carrier mobilities in crystalline silicon *Sol. Energy Mater. Sol. Cells* **131** 92–99
[65] Kunst M and Beck G 1986 The study of charge carrier kinetics in semiconductors by microwave conductivity measurements *J. Appl. Phys.* **60** 3558–66
[66] Buczkowski A, Radzimski Z J, Rozgonyi G A and Shimura F 1992 Separation of the bulk and surface components of recombination lifetime obtained with a single laser/microwave photoconductance technique *J. Appl. Phys.* **72** 2873–8
[67] Semilab (available at: https://semilab.com/category/products/carrier-lifetime-u-pcd-qss-upcd-0)
[68] Freiberg Instruments (available at: https://www.freiberginstruments.com/upcdmdp/mdpmap.html)
[69] Schöfthaler M and Brendel R 1995 Sensitivity and transient response of microwave reflection measurements *J. Appl. Phys.* **77** 3162–73
[70] Macdonald D and Cuevas A 2003 Validity of simplified Shockley-Read-Hall statistics for modeling carrier lifetimes in crystalline silicon *Phys. Rev.* B **67** 1–7
[71] Macdonald D and Cuevas A 1999 Trapping of minority carriers in multicrystalline silicon *Appl. Phys. Lett.* **74** 1710–2
[72] Schmidt J, Bothe K and Hezel R 2002 Oxygen-related minority-carrier trapping centers in p-type Czochralski silicon *Appl. Phys. Lett.* **80** 4395–7
[73] Macdonald D, Sinton R A and Cuevas A 2001 On the use of a bias-light correction for trapping effects in photoconductance-based lifetime measurements of silicon *J. Appl. Phys.* **89** 2772–8
[74] Hu Y, Schøn H, Nielsen Ø, Johannes Øvrelid E and Arnberg L 2012 Investigating minority carrier trapping in n-type Cz silicon by transient photoconductance measurements *J. Appl. Phys.* **111** 053101
[75] Zhu Y, Juhl M K, Coletti G and Hameiri Z 2019 Reassessments of minority carrier traps in silicon with photoconductance decay measurements *IEEE J. Photovolt.* **9** 652–9
[76] Neuhaus D H, Cousins P J and Aberle A G 2003 Trapping and junction-related perturbations of the effective excess carrier lifetime *3rd World Conf. on Photovoltaic Energy Conversion* pp 91–94
[77] Cousins P J, Neuhaus D H and Cotter J E 2004 Experimental verification of the effect of depletion-region modulation on photoconductance lifetime measurements *J. Appl. Phys.* **95** 1854–8
[78] Trupke T, Bardos R A and Abbott M D 2005 Self-consistent calibration of photoluminescence and photoconductance lifetime measurements *Appl. Phys. Lett.* **87** 184102
[79] Giesecke J A, Schubert M C, Warta W, Giesecke J A, Schubert M C and Warta W 2012 Measurement of net dopant concentration via dynamic photoluminescence *J. Appl. Phys.* **112**
[80] Giesecke J A, Schubert M C and Warta W 2012 Self-sufficient minority carrier lifetime in silicon from quasi steady state photoluminescence *Phys. Status Solidi* a **209** 2286–90
[81] Giesecke J A, Glunz S W and Warta W 2013 Understanding and resolving the discrepancy between differential and actual minority carrier lifetime *J. Appl. Phys.* **113** 073706
[82] Bardos R A, Trupke T, Schubert M C and Roth T 2006 Trapping artifacts in quasi-steady-state photoluminescence and photoconductance lifetime measurements on silicon wafers *Appl. Phys. Lett.* **88** 1–3
[83] Heinz F D, Giesecke J, Mundt L E, Kasemann M, Warta W and Schubert M C 2015 On the implication of spatial carrier density non-uniformity on lifetime determination in silicon *J. Appl. Phys.* **118**
[84] Herlufsen S, Hinken D, Offer M, Schmidt J and Bothe K 2013 Validity of calibrated photoluminescence lifetime measurements of crystalline silicon wafers for arbitrary lifetime and injection ranges *IEEE J. Photovolt.* **3** 381–6
[85] Bowden S and Sinton R A 2007 Determining lifetime in silicon blocks and wafers with accurate expressions for carrier density *J. Appl. Phys.* **102** 124501
[86] Sinton R A and Trupke T 2012 Limitations on dynamic excess carrier lifetime calibration methods *Prog. Photovolt., Res. Appl.* **20** 246–9
[87] Giesecke J A and Warta W 2014 Understanding carrier lifetime measurements at nonuniform recombination *Appl. Phys. Lett.* **104** 082103
[88] Phang S P, Sio H C and Macdonald D 2016 Applications of carrier de-smearing of photoluminescence images on silicon wafers *Prog. Photovolt., Res. Appl.* **24** 1547–53
[89] Sio H C, Phang S P, Trupke T and Macdonald D 2014 An accurate method for calibrating photoluminescence-based lifetime images on multi-crystalline silicon wafers *Sol. Energy Mater. Sol. Cells* **131** 77–84
[90] Zhu Y, Heinz F D, Juhl M, Schubert M C, Trupke T and Hameiri Z 2018 Photoluminescence imaging at uniform excess carrier density using adaptive nonuniform excitation *IEEE J. Photovolt.* **8** 1787–92
[91] WCT-120 - Sinton Instruments (available at: https://www.sintoninstruments.com/products/wct-120/)
[92] Giesecke J 2014 *Quantitative Recombination and Transport Properties in Silicon from Dynamic Luminescence* (Berlin: Springer)
[93] Höffler H, Schindler F, Brand A, Herrmann D, Eberle R, Post R, Kessel A, Greulich J and Schubert M C 2020 Review and recent development in combining photoluminescence- and electroluminescence-imaging with carrier lifetime measurements via modulated photoluminescence at variable temperatures *37th European Photovoltaic Solar Energy Conf. and Exhibition* pp 264–76
[94] Giesecke J A and Warta W 2012 Microsecond carrier lifetime measurements in silicon via quasi-steady-state photoluminescence *Prog. Photovolt., Res. Appl.* **20** 238–45
[95] Paudyal B B, McIntosh K R, Macdonald D H, Richards B S and Sinton R A 2008 The implementation of temperature control to an inductive-coil photoconductance instrument for the range of 0–230°C *Prog. Photovolt., Res. Appl.* **16** 609–13

[96] Paudyal B B 2010 Temperature and injection dependent lifetime spectroscopy for defect characterization in silicon *PhD Thesis* Australian National University, Canberra
[97] Zhu Y 2020 Advanced characterization of defects in silicon wafers and solar cells *PhD Thesis* University of New South Wales, Sydney
[98] Zhu Y, Rougieux F, Grant N E, Guzman J A T D, Murphy J D, Markevich V P, Coletti G, Peaker A R and Hameiri Z 2020 Electrical characterization of thermally activated defects in n-type float-zone silicon *IEEE J. Photovolt.* **11** 26–35
[99] Couderc R, Amara M and Lemiti M 2014 Reassessment of the intrinsic carrier density temperature dependence in crystalline silicon *J. Appl. Phys.* **115** 093705
[100] Green M A 1990 Intrinsic concentration, effective densities of states, and effective mass in silicon *J. Appl. Phys.* **67** 2944–54
[101] Pässler R 2002 Dispersion-related description of temperature dependencies of band gaps in semiconductors *Phys. Rev.* B **66** 85201
[102] Schenk A 1998 Finite-temperature full random-phase approximation model of band gap narrowing for silicon device simulation *J. Appl. Phys.* **84** 3684–95
[103] Bernardini S, Naerland T U, Coletti G and Bertoni M I 2018 Defect parameters contour mapping: a powerful tool for lifetime spectroscopy data analysis *Phys. Status Solidi* b **255** 1800082
[104] Bernardini S, Naerland T U, Blum A L, Coletti G and Bertoni M I 2017 Unraveling bulk defects in high-quality c-Si material via TIDLS *Prog. Photovolt., Res. Appl.* **25** 209–17
[105] Narland T U, Bernardini S, Wiig M S and Bertoni M I 2018 Is it possible to unambiguously assess the presence of two defects by temperature-and injection-dependent lifetime spectroscopy? *IEEE J. Photovolt.* **8** 465–72
[106] Nampalli N, Fung T H, Wenham S, Hallam B and Abbott M 2017 Statistical analysis of recombination properties of the boron-oxygen defect in p-type Czochralski silicon *Front. Energy* **11** 4–22
[107] Zhu Y, Le Gia Q T, Juhl M K, Coletti G and Hameiri Z 2017 Application of the Newton–Raphson method to lifetime spectroscopy for extraction of defect parameters *IEEE J. Photovolt.* **7** 1092–7
[108] Voronkov V V, Falster R, Bothe K, Lim B and Schmidt J 2011 Lifetime-degrading boron-oxygen centres in p-type and n-type compensated silicon *J. Appl. Phys.* **110** 063515
[109] Voronkov V V, Falster R J, Schmidt J, Bothe K and Batunina A 2010 Lifetime degradation in boron doped czochralski silicon *ECS Trans.* **33** 103–12
[110] Raphson J 1702 *Analysis Aequationum Universalis* (London: Typis Tho. Braddyll)
[111] Buratti Y, Le Gia Q T, Dick J, Zhu Y and Hameiri Z 2020 Extracting bulk defect parameters in silicon wafers using machine learning models *npj Comput. Mater.* **6** 1–8
[112] Mundt L E, Schubert M C, Schon J, Michl B, Niewelt T, Schindler F and Warta W 2015 Spatially resolved impurity identification via temperature-and injection-dependent photoluminescence imaging *IEEE J. Photovolt.* **5** 1503–9
[113] Hameiri Z, Juhl M K, Carlaw R and Trupke T 2015 Spatially resolved lifetime spectroscopy from temperature-dependent photoluminescence imaging *42nd IEEE Photovoltaic Specialist Conf.* pp 1–3
[114] Schön J *et al* 2016 Identification of lifetime limiting defects by temperature- and injection-dependent photoluminescence imaging *J. Appl. Phys.* **120** 105703
[115] Haug H, Søndenå R, Berg A and Wiig M S 2019 Lifetime spectroscopy with high spatial resolution based on temperature- and injection dependent photoluminescence imaging *Sol. Energy Mater. Sol. Cells* **200** 109994
[116] Coletti G, Manshanden P, Bernardini S, Bronsveld P C P C P, Gutjahr A, Hu Z and Li G 2014 Removing the effect of striations in n-type silicon solar cells *Sol. Energy Mater. Sol. Cells* **130** 647–51
[117] Geerligs L J and Macdonald D 2004 Dynamics of light-induced FeB pair dissociation in crystalline silicon *Appl. Phys. Lett.* **85** 5227–9
[118] Macdonald D H, Geerligs L J and Azzizi A 2004 Iron detection in crystalline silicon by carrier lifetime measurements for arbitrary injection and doping *J. Appl. Phys.* **95** 1021–8
[119] Conzelmann H, Graff K and Weber E R 1983 Chromium and chromium-boron pairs in silicon *Appl. Phys.* A **30** 169–75
[120] Ramspeck K, Zimmermann S, Nagel H, Metz A, Gassenbauer Y, Birkmann B and Seidl A 2012 Light induced degradation of rear passivated mc-Si solar cells *27th European Photovoltaic Solar Energy Conf. and Exhibition* pp 861–5
[121] Juhl M K, Heinz F D, Coletti G, Macdonald D, Rougieux F E, Schindle F, Niewelt T, Schubert M C and Ise F 2018 An open source based repository for defects in silicon *7th World Conf. on Photovoltaic Energy Conversion* pp 0328–32
[122] Rougieux F E, Sun C and Macdonald D 2018 Determining the charge states and capture mechanisms of defects in silicon through accurate recombination analyses: a review *Sol. Energy Mater. Sol. Cells* **187** 263–72
[123] Sah C and Shockley W 1958 Electron-hole recombination statistics in semiconductors through flaws with many charge conditions *Phys. Rev.* **109** 1103–15
[124] Macdonald D, Brendle W, Cuevas A and Istratov A A 2002 Injection-dependent lifetime studies of copper precipitates in silicon *12th Workshop on Crystalline Silicon Solar Cell Materials and Processes*
[125] Warta W 2006 Advanced defect and impurity diagnostics in silicon based on carrier lifetime measurements *Phys. Status Solidi* a **203** 732–46
[126] Rougieux F E, Grant N E, Barugkin C, Macdonald D and Murphy J D 2015 Influence of annealing and bulk hydrogenation on lifetime-limiting defects in nitrogen-doped floating zone silicon *IEEE J. Photovolt.* **5** 495–8
[127] Zhu Y, Coletti G and Hameiri Z 2019 Injection dependent lifetime spectroscopy for two-level defects in silicon *IEEE 46th Photovoltaic Specialists Conf.* pp 0829–32
[128] Zhu Y, Sun C, Niewelt T, Coletti G and Hameiri Z 2020 Investigation of two-level defects in injection dependent lifetime spectroscopy *Sol. Energy Mater. Sol. Cells* **216** 110692